



Published in final edited form as:

Lab Chip. 2019 April 23; 19(9): 1579–1588. doi:10.1039/c9lc00173e.

## Traction microscopy with integrated microfluidics: responses of the multi-cellular island to gradients of HGF

Hwanseok Jang<sup>‡,a</sup>, Jongseong Kim<sup>‡,a</sup>, Jennifer H. Shin<sup>b</sup>, Jeffrey J. Fredberg<sup>c</sup>, Chan Young Park<sup>c</sup>, Yongdoo Park<sup>a</sup>

<sup>a</sup>Department of Biomedical Sciences, College of Medicine, Korea University, Seoul 02841, Republic of Korea.

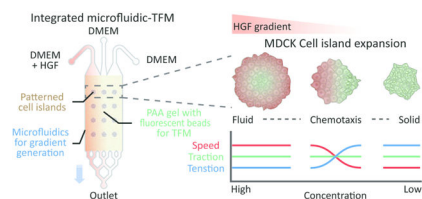
<sup>b</sup>Department of Mechanical Engineering, Korea Advanced Institute of Science and Technology, Daejeon 34141, Republic of Korea.

<sup>c</sup>Department of Environmental Health, Harvard School of Public Health, Boston, MA 02115, USA.

### Abstract

Collective cellular migration plays central roles in development, regeneration, and metastasis. In these processes mechanical interactions between cells are fundamental, but measurement of these interactions is often hampered by technical limitations. To overcome some of these limitations here we describe a system that integrates microfluidics with traction force microscopy (TFM). Using this system we can measure simultaneously, and in real time, cellular migration speeds, traction forces, and intercellular tension throughout a multicellular confluent island of confluent Madin-Darby canine kidney (MDCK) cells. The cell island is exposed to hepatocyte growth factor (HGF) at controlled concentrations and controlled gradients; HGF is known to elicit epithelial-to-mesenchymal transition (EMT) and cell scattering. As expected, the rate of expansion of the cell island was dependent on the concentration of HGF. Higher concentrations of HGF reduced intercellular tensions, as expected during EMT. A novel finding, however, is that the effects of HGF concentration and its gradient were seen to be cooperative. This integrated experimental system thus provides an improved window to better understand cellular forces during collective cellular migration and EMT.

### Graphical Abstract



cypark@hsph.harvard.edu, ydpark67@korea.ac.kr.

<sup>‡</sup>Co-first authors.

Conflicts of interest

There are no conflicts to declare.

## Introduction

Collective cellular migration is fundamental to tissue formation,<sup>1, 2</sup> immune response,<sup>3, 4</sup> wound healing,<sup>5, 6</sup> angiogenesis<sup>7, 8</sup> and metastasis.<sup>9–11</sup> Lab-on-a-chip technologies, including microfluidic cell culture,<sup>12, 13</sup> organs-on-a-chip,<sup>14, 15</sup> and microarrays,<sup>16, 17</sup> help to provide better understanding, but thus far have not addressed the phenomenon of collective cellular migration. To study collective cellular migration *in vitro*, we therefore sought to develop a microphysiological system with precise control of physiochemical stimuli and simultaneous monitoring of responses in real time.

For cells to move collectively, both regulation and sensing of the microenvironment are essential.<sup>18–20</sup> For instance, cells perceive physicochemical stimuli and respond by changing the cell motility,<sup>21</sup> cell-substrate interactions,<sup>22, 23</sup> and cell-cell interactions,<sup>24</sup> resulting in cooperative cell migration with a specific directionality.<sup>25–27</sup> Hepatocyte growth factor (HGF), for example, is an example of a stimulus that causes cells to attenuate cell-cell interactions and enhance cell motility in a process known as epithelial to mesenchymal transition (EMT).<sup>28–31</sup> Previous studies have shown that HGF, which is also known as a scattering factor, induces cellular EMT in an epithelial cell monolayer in a dose-dependent manner.<sup>32, 33</sup>

Here we describe a multichannel microfluidic system that enables the generation of a concentration gradient of HGF in flow, facilitating the cooperative migration of Madin-Darby canine kidney (MDCK) cell clusters. By incorporating traction force microscopy (TFM) into the system, we were able to identify the cellular motility, tension, and traction forces caused in response to HGF. We demonstrate that MDCK cells in a circular cluster develop enhanced responses in a concentration-dependent and gradient-dependent manner. We also found that responses are associated with junction proteins, including vinculin, E-cadherin, and F-actin, each of which participates in cell adhesion, migration, and EMT. These results suggest that our microfluidic TFM system is applicable to exploring many open questions in the field of cooperative cellular migration under a chemical gradient of soluble factors.

## Results

### Integrated microfluidic system with TFM

To explore the collective migration of cell clusters in response to the concentration gradient of a chemical, we integrated a microfluidic system with TFM by enveloping a fluorescent bead-embedded polyacrylamide (PAA) gel with a polydimethylsiloxane (PDMS) microchannel structure (Fig. 1a). As a model cell system, MDCK cells were seeded on the PAA gels in the presence of a PDMS stencil with circular holes which allowed the formation of cell monolayers with a confined size and shape.<sup>33</sup> Twelve islands of MDCK cell clusters (3 columns by 4 rows, and each island had a diameter of 800  $\mu\text{m}$ ) were prepared. After cells attached on PAA gels, the stencil was gently removed and microchannel structure was put over the PAA gels to produce closed channel over cell clusters. A stable laminar flow within the microchannel was established by applying negative pressure using a syringe pump to the outlet of a hierarchically structured tree-like channel (Fig. 1b). To develop a concentration

gradient, the left inlet was supplied with 20 ng/ml HGF-containing media, while the middle and right inlets were supplied with media without HGF. The entire assembly was put on a microscope enclosed in an incubator at 37 °C and 5% CO<sub>2</sub> (Fig. 1c).

### The effect of an HGF concentration gradient on MDCK cell migration

The expansion of MDCK cell islands was monitored in response to the HGF concentration and its gradient (Fig. 2a). Rhodamine-conjugated dextran (R-dextran), which has a molecular weight similar to HGF, was used to estimate spatiotemporal distribution of HGF with the microfluidic channel (Fig. 2b). The fluorescence intensity of R-dextran showed that the concentration decreased from left to right, yielding concentration gradients over the array of cell islands (Fig. 2c). The degree of the concentration gradient was tunable by adjusting the flow rate of target molecules (Fig. S1a and b<sup>†</sup>). Notably, after stabilization of flow, the concentration gradients were fairly consistent and within 5% variation over the course of 8 hr measurements (Fig. S1c<sup>†</sup>). Based on the HGF concentrations, the cell islands were divided into three regions; left (high), middle (medium) and right (low) (Fig. 2c).

The expansion of each MDCK cell island was observed by bright field microscopy in the presence of HGF in the microfluidic TFM system. As HGF is known to induce scattering of epithelial cells,<sup>30, 34–35</sup> MDCK cell islands expanded more when HGF concentration was higher (Fig. 2d). The islands on the left columns where HGF concentration was high expanded more than the islands on the right columns where HGF concentration was low. The expansion of those islands in the middle column was in between the left and the right. When we compared the boundaries of islands between 0 min and 500 min, it was evident that the degree of expansion was dependent on HGF concentration. Moreover, we found that in the middle island in which the HGF gradient is most steep, the left half of the island expanded more than the right half of the island and thus showed the asymmetric expansion within an island (Fig. 2e). The trajectory of cell locomotion confirmed the asymmetric migration of those cells in the middle island (Fig. 2f).

### Spatiotemporal distribution of cell migration, traction and tension in the MDCK cell islands

During the expansion of MDCK cell islands over 500 min, velocity of cell migration, cellular contractile force on substrate and intercellular stress were analyzed. The magnitude of velocity, speed is shown by color-coded maps where the red color indicates outward movements and the blue color indicates the inward movements (Fig. 3a). At the beginning of the expansion, all three islands showed similar pattern of speed distribution with a shallow red rim along the boundary indicating that the migration happened mostly on the boundary of the island. After 500 min of exposure to HGF gradients, however, the patterns of speed distribution were different among 3 islands. On the left island where HGF concentration was high, most of cells in the island were moving outward. On the right island where HGF concentration was low, overall speed was smaller than the left island. On the middle island where HGF gradient was most steep, the left half of island migrated more while there was minimal migration on the right half. Thus there was asymmetric pattern of migration in the middle island. When we compared the average speed in each island, the left island was

<sup>†</sup>Electronic Supplementary Information (ESI) available. See DOI: [10.1039/x0xx00000x](https://doi.org/10.1039/x0xx00000x)

always fast moving than the others and there was peak at 2hr (Fig. 3b). Next, we compared the traction distribution. Unlike the speed distribution, there was no clear difference among the islands (Fig. 3c and d). Using monolayer stress microscopy, we computed intercellular stress. Again, at the beginning of the expansion, there was no difference among island but after 500 min exposure to HGF gradient, the intercellular stress of the left island was visibly smaller than the other islands (Fig. 3e). The middle island showed less tension on the left half than the right. Also, we found that the average tension within the left island decreased after 3hr of exposure while there were little changes in the other 2 islands (Fig. 3f).

### **Differential migratory behaviors of the MDCK cell islands in response to the HGF concentration and its gradient.**

The migratory behavior of MDCK cell islands was characterized by the HGF concentration and its gradient. Therefore, we divided each island by left and right semicircles, where the HGF concentration gradually decreased from the left to the right, as shown in Fig. 4a (solid blue lines). The gradient in the sectioned area was also estimated, which showed substantial values of 0.55 and 0.51 a.u. for zones 2 and 3, respectively, while other zones were fairly stable (less than 0.1 a.u.) for changes in the HGF concentration (Fig. 4a, red bars). The cellular speed of each semicircle was measured by averaging all the components in the area, resulting in a positive correlation with the HGF concentration. This result indicated that HGF favors the migration of cells, in which a higher concentration causes a faster speed. Strikingly, the speed of zone 2 showed the highest value, although the concentration was lower than that of zone 1. This result suggested that the HGF gradient may contribute to enhancing the cell speed of zone 2, where the gradient significantly differed by 28-fold compared to that of zone 1. This behavior was clearly observable in the middle column (zones 3 and 4), which showed a 1.8-fold increase in the cellular speed in zone 3 compared to that in zone 4. The change in average traction was little to none with each island though the left island (zones 1 and 2) showed slightly less traction than the other islands (Fig. 4c). We also found that the average cellular tension in each zone was inversely correlated with the local HGF concentrations (Fig. 4d), while the effect of the HGF gradient was negligible. With all together, our results suggest that the effects of HGF concentration and its gradient could be cooperative primarily on cellular speed rather than the tension and traction.

### **The HGF concentration gradient induces asymmetric distribution of actin, focal adhesions (FAs), and adherens junctions (AJs) within the MDCK cell islands**

To determine whether the HGF gradient made any change in cytoskeleton or cell junctions, after 500 min exposure to HGF gradient, we stained F-actin, E-cadherin and vinculin in the cells in one of the middle islands and magnified representative regions from left and right halves (Fig. 5a). First, we found that cells of the left half were thinner than those on the right half (Fig. 5b – d). The localization of the proteins in the cell island was carefully investigated for both the FA and AJ regions along the z-axis. On the left side, where the HGF concentration was high, E-cadherins were rarely observed in the cellular AJ junction as a thin line (Fig. 5e), and cortical F-actin fibers were stretched between distinct vinculin spots surrounding the cell boundary at the FA region (Fig. 5g). Vinculins were not only located at the cell junction with other proteins but also evenly spread over the entire area of cells. However, on the right side where the HGF concentration was low, thick and distinct actin

bundles were located along the cell junctions with clear lines of E-cadherin (Fig. 5f and h). E-cadherin-F-actin-vinculin complexes developed thick and distinct bands along the cell junctions at the AJ region (Fig. 5f), while vinculins were uniformly distributed in the area of cells at the FA region (Fig. 5h). The results indicated that the force-related protein complexes were asymmetrically distributed in the cell island along with the HGF concentration and its gradient, which is physically connected to breaking the balance of collective migration, tensile force, and morphology of a cell monolayer.

## Discussion and conclusion

Collective cellular migration in the presence of chemokines is one of the important biological events in development,<sup>27, 29</sup> regeneration,<sup>5, 28</sup> and metastasis.<sup>34, 35</sup> The mechanism by which collective cell migration is mediated remains to be explained by the dynamics of cell-cell junctions and cell-substrate interactions.<sup>36, 37</sup> In this study, we developed an integrated microfluidic TFM system with patterned cell islands that can not only regulate the chemical concentration with gradients but also evaluate the cellular behavior with kinematics and force mapping *in situ*. Our experimental setup offers a number of advantages over previous microfluidics systems for studying cell migration. The complex *in vivo* tissue microenvironment is incorporated with patterned MDCK cell collectives, and the size and shape of the islands are controllable, allowing for the evaluation of physicochemical effects on collective cellular migration. The integrated TFM system provides further advantages. Previous studies of cell migration have been mostly conducted on single-cell behavior imbedded in the TFM system,<sup>32, 38, 39</sup> but these studies did not evaluate the collectiveness and dynamics of cell groups. The application of flow and a gradient of a molecule of interest in our setup is pivotal to understanding the chemotactic influence on cellular functions, including EMT,<sup>40</sup> metastasis,<sup>34</sup> and stem cell homing.<sup>41</sup> In the microfluidic TFM system, cellular speed, traction, and tension within groups of cell monolayers are all measurable under various concentrations of the growth factor HGF and its gradient in a spatiotemporal manner.

The conversion of epithelial cells to cells with mesenchymal-like characteristics is a crucial step not only for wound healing but also for cancer progression,<sup>31, 34</sup> where epithelial cells lose apicobasal polarity and cell-cell interactions.<sup>30, 40, 42–44</sup> At the molecular level, EMT is accompanied by the loss of the E-cadherin complex at AJs, resulting in reinforcement of FAs through vinculin.<sup>30, 33</sup> Although the mechanism by which EMT occurs has been extensively studied, the biophysical characteristics of the epithelial cell layer in an *in vivo*-like environment remain to be answered. Our finding that a collective migration of MDCK cells depends on the HGF concentration as well as its gradient is unprecedented for cell migration and thus EMT. Typically, cells migrate toward higher concentrations of soluble factors, which is known as chemotaxis; however HGF increased the expansion of MDCK cell islands without chemotactic directionality and induced EMT.<sup>32, 45, 46</sup> The highest speed of the cell groups was observed once the concentration and gradient of HGF were coapplied to the system. Traction generated by the cell groups was fairly consistent under various concentrations of HGF in solution, suggesting that the cells maintained group collectiveness.<sup>37, 47</sup> Tension measured in the cell groups was shown to be inversely associated with the HGF concentration, and there was no influence by the gradient, unlike the cell speed.

Our finding using the microfluidic TFM system has important physiological implications for how MDCK cells sense secreted HGFs and efficiently activate collective cell migration and EMT. Since cells experience increases or decreases in the HGF concentration *in vivo*,<sup>28, 29, 45</sup> our results are consistent with the model showing that the HGF concentration and its gradient cooperate to initiate collective cell migration in the process of EMT. Immunostaining of F-actin, E-cadherin, and vinculin further provided evidence of EMT development induced by HGF.<sup>48–50</sup> Interestingly, the application of the HGF gradient within a single cell island induced asymmetric cellular dynamics in relation to EMT, while the fluid- and the solid-like states of cell collectives were observed at higher and lower HGF concentrations, respectively, in the same microfluidic chip. The characteristics of EMT at the interface between higher and lower HGF concentrations were further confirmed by the lower cellular tension and higher speed in only a part of the asymmetric cell island.

Although only the effects of HGF on the collective migration of MDCK cells were studied in the current study, the results suggest that the microfluidic TFM system has capabilities to investigate many remaining questions in the field of mechanobiology. For instance, how cells sense external stimuli and translate these stimuli to mechanical output is fundamental for a better understanding of cellular functions. In addition, biophysical analysis of cell collectives rather than individual cells is highly necessary to enhance the existing knowledge of physiology and pathology.

## Experimental

### Cell culture

MDCK (strain II) cells were cultured in low-glucose Dulbecco's modified Eagle's media (DMEM; Welgene, Korea) supplemented with 10% (v/v) fetal bovine serum (FBS; Gibco, USA) and 1% (v/v) antibiotic-antimycotic (Gibco). The cells were maintained in a humidified incubator (Panasonic, Japan) at 37 °C and 5% CO<sub>2</sub>.

### Fabrication of a PDMS stencil and microchannel component

A PDMS stencil for cell patterning and a microchannel component for gradient generation were fabricated by general soft lithography using PDMS (Sylgard 184; Dow Corning, USA) based on a method reported in previous studies.<sup>33, 41</sup> Briefly, a well-mixed PDMS pre-cured solution with a 10:1 ratio of prepolymer to curing agent was poured onto SU-8 master molds (Outsourced; MicroFIT, Korea) at a thickness of 200 μm for the stencils and 3 mm for the microchannel parts and was cured in a drying oven at 85 °C for 2 hours. After curing, the thin PDMS films with holes (diameter = 700 μm) were trimmed with a 14-mm-diameter punch, and the channel parts were trimmed to 24 mm by 24 mm. The resulting PDMS stencils and chips were autoclaved.

### Preparation of a polyacrylamide (PAA) gel substrate

Based on a previous protocol,<sup>33</sup> 1 ml of PAA gel solution (6 kPa) consisted of 135 μl of 40% acrylamide (Bio-Rad, USA), 101 μl of 2% *N,N'*-Methylenebis(acrylamide) (BIS) solution (Bio-Rad, USA), 658 μl of highly purified water, 5 μl of green fluorescent beads (diameter =

500 nm; FluoSpheres; Invitrogen, USA), 100  $\mu$ l of 0.5% (w/v) ammonium persulfate (Bio-Rad, USA) and 1  $\mu$ l of tetramethylethylenediamine (TEMED) (Bio-Rad, USA).

A glass chip with a rectangular groove with a depth of 100  $\mu$ m for filling a soft substrate with a constant height was custom prepared (MicroFIT) (Fig. 1a (i)). After autoclaving the glass chips, the grooves were treated with a bind-silane solution consisting of 0.04% (v/v) acetic acid and 0.025% (v/v) silane A174 (3-(trimethoxysilyl)propyl methacrylate; Sigma-Aldrich, USA) diluted with highly purified water at room temperature for 1 hour. The glass chips were then rinsed with highly purified water three times and dried.

The prepared PAA gel solution was filled into the grooves and flattened by cover glasses (diameter = 18 mm, Marienfeld, Germany). To align the fluorescent beads along the upper surface of the gel, the glass chips filled with PAA gel solution were turned upside-down and centrifuged at 700 rpm for 10 min. After 50 min for polymerization of the PAA gel, highly purified water was poured on top of the glass chips, and the cover glasses were removed (Fig. 1a (ii)).

### Cell patterning on the PAA gel

The PAA gel surface was functionalized with Sulfo-SANPAH (sulphosuccin-imidyl-6-(4-azido-2-nitrophenylamino) hexanoate; 1 mg/ml in 50 mM HEPES buffer; Thermo Scientific Pierce, USA) and activated by ultraviolet (UV) light (365 nm wavelength) for 10 min. The gel surfaces were then washed with 0.1 M HEPES (Sigma-Aldrich, USA) twice and with phosphate-buffered saline (PBS; Welgene, Korea) once. The functionalized PAA gels were coated with 100  $\mu$ g/ml collagen type I (rat tail; Corning, USA) diluted with PBS at 4  $^{\circ}$ C overnight. One day later, the collagen solution was removed, and the glass chips with the PAA gel were rinsed with PBS three times.

The autoclaved PDMS stencils were coated with 2% Pluronic F-127 solution (Sigma-Aldrich) diluted with PBS, incubated at 37  $^{\circ}$ C 1 hour and then rinsed with PBS three times. The stencil was placed on the surface of the collagen-coated PAA gel after removing the liquid from the stencil and PAA gel (Fig. 1a (iii)). The holes in the PDMS stencil were filled with PBS without air bubbles and covered with a 200  $\mu$ l droplet of MDCK cells suspended in medium (density =  $2 \times 10^6$  cells/ml). After the sample was incubated at 37  $^{\circ}$ C and 5% CO<sub>2</sub> for 1 hour to attach the cells onto the PAA gel surface, the PDMS stencil was gently washed with DMEM twice and carefully removed. The medium was then exchanged with fresh DMEM to remove cell debris and develop the patterned MDCK cell monolayer islands (Fig. 1a (iv)).

### Integration of the microfluidic TFM system

The channel-engraved surface of the autoclaved PDMS chip was treated with O<sub>2</sub> plasma (Femto Science, Korea). After removing the water from the glass chip where the cells were patterned, the plasma-treated PDMS chip was placed on top of the glass chip, and the two chips were fixed together by a customized cast (Han-Gug Mechatronics, Korea) (Fig. 1a (v) and c). Three 200-micron tips (Axygen, USA) filled with media were inserted into the three inlet ports, and a 2 ml syringe (KOVAX, Korea) was connected to the outlet port through a modified 18 G needle (KOVAX, Korea), a 75-cm-long mini-volume line (Hyupsung, Korea),

and a 3-way stopcock extension tube (Hyupsung). After replacing the media in the leftmost inlet with DMEM supplemented with 20 ng/ml recombinant human HGF (Sigma-Aldrich, USA) and 1 mg/ml rhodamine B isothiocyanate-dextran (70 kDa; Sigma-Aldrich, USA), the fluid was withdrawn via the outlet using a syringe pump (Chemyx, USA) at a rate of 0.1  $\mu$ l/min.

### Time-lapse microscopy

Every experiment was performed on a JuLI stage live cell imaging system (NanoEnTek, Korea) with a 4 $\times$  objective lens (Olympus, Japan) in a cell culture incubator. Bright field was used to image the cells, a green fluorescent protein (GFP) filter was used to image the fluorescent beads, and a red fluorescent protein (RFP) filter was used to image rhodamine B isothiocyanate-dextran. Images were acquired every 10 min for 12 hours. At the last timepoint, the cells were trypsinized to obtain an image of the reference bead position that the substrate stress was relaxed from the cellular physical force.

### Quantification analysis

The obtained bright field cell images and fluorescent bead and dextran images were numerically converted and quantitatively analyzed using a customized source code developed with MATLAB (MathWorks Inc., USA). The calculation and analytical code used in this study was based on previous studies conducted by the Fredberg group from the Harvard T.H. Chan School of Public Health.<sup>51–53</sup> Briefly, the images at each timepoint were analyzed for cell and bead displacement through particle image velocimetry (PIV) based on normalized cross-correlation between a cell image and the respective previous cell image or between a bead image and the reference bead image. The displacement result from the cell images was converted to a movement trajectory and velocity of the cells, and the displacement result from the bead images was converted to the traction force using unconstrained Fourier transform traction microscopy (FTTM). The traction data were used to calculate intercellular stress, especially tension, using monolayer stress microscopy (MSM). The dextran images were normalized to the maximum and minimum values of the pixel intensity and used to infer the HGF concentration and its gradient.

### Immunofluorescence assay

After 9 hours of monitoring the expansion of the MDCK cellular islands, the cells were fixed with 4% paraformaldehyde in PBS for 20 min. The cells were permeabilized with 0.4% Triton X-100 in PBS for 20 min and blocked with 5% bovine serum albumin (BSA) in phosphate-buffered saline Tween-20 (PBST) for 30 min. To detect the expression positions of E-cadherin and vinculin, monoclonal anti-E-cadherin (1:50 dilution; Cell Signaling Technologies, USA) and monoclonal anti-vinculin (1:400 dilution; Sigma-Aldrich, USA) were used and incubated on the samples for 1 hour. After washing with PBST 5 times, the cells were incubated with Alexa Fluor 594 anti-rabbit IgG (1:50 dilution; Abcam, USA), Alexa Fluor 488 anti-mouse (1:400 dilution; Abcam, USA), and Alexa Fluor 350 phalloidin (1:25 dilution; Life Technologies, USA) for 1 hour. After washing the samples, fluorescent mounting medium (Dako, USA) was added dropwise, and a cover glass (diameter = 12 mm; Marienfeld, Germany) was placed on top of the sample. Fluorescent images of the entire MDCK cell island were captured by a fluorescence microscope (Axioscope; Carl Zeiss,

Germany) equipped with a 40× objective lens. To identify the FA and AJ regions, a confocal microscope (LSM 510, Carl Zeiss) was used, and 15~20 images at 100 nm intervals along the z-axis were acquired. Using ImageJ (NIH, USA), we stitched the high-resolution images to compose an image of an entire cell island and merged the confocal images at the basal or mid-apical sections through maximal intensity projections of 4~5 slides.

## Supplementary Material

Refer to Web version on PubMed Central for supplementary material.

## Acknowledgements

We thank numerous colleagues who provided insightful help with the preparation in this MS. Special thanks to Prof. H. Chun at Korea University, Dr. B. Gweon at Hanyang University, and Mr. Y. Cho at KAIST for the supply of experimental materials. This work was supported by the National Research Foundation of Korea (NRF) grant funded by the Korea government (MSIP) (No. NRF-2017R1E1A1A01075103), Korea University Grant, and the BK 21 Plus program.

## References

1. Chuai M, Hughes D and Weijer CJ, *Curr Genomics*, 2012, 13, 267–277. [PubMed: 23204916]
2. Raza Q and Jacobs JR, *Dev Biol*, 2016, 419, 285–297. [PubMed: 27618756]
3. Luster AD, Alon R and von Andrian UH, *Nat Immunol*, 2005, 6, 1182–1190. [PubMed: 16369557]
4. Schumann K, Lammermann T, Bruckner M, Legler DF, Polleux J, Spatz JP, Schuler G, Forster R, Lutz MB, Sorokin L and Sixt M, *Immunity*, 2010, 32, 703–713. [PubMed: 20471289]
5. Poujade M, Grasland-Mongrain E, Hertzog A, Jouanneau J, Chavrier P, Ladoux B, Buguin A and Silberzan P, *Proc Natl Acad Sci U S A*, 2007, 104, 15988–15993. [PubMed: 17905871]
6. Anon E, Serra-Picamal X, Hersen P, Gauthier NC, Sheetz MP, Trepat X and Ladoux B, *Proc Natl Acad Sci U S A*, 2012, 109, 10891–10896. [PubMed: 22711834]
7. Vitorino P, Hammer M, Kim J and Meyer T, *Mol Cell Biol*, 2011, 31, 342–350. [PubMed: 20974808]
8. Costa G, Harrington KI, Lovegrove HE, Page DJ, Chakravartula S, Bentley K and Herbert SP, *Nat Cell Biol*, 2016, 18, 1292–1301. [PubMed: 27870831]
9. Friedl P, Locker J, Sahai E and Segall JE, *Nat Cell Biol*, 2012, 14, 777–783. [PubMed: 22854810]
10. Matisse LA, Palmer TD, Ashby WJ, Nashabi A, Chytil A, Aakre M, Pickup MW, Gorska AE, Zijlstra A and Moses HL, *Breast Cancer Res*, 2012, 14, R98. [PubMed: 22748014]
11. Wu Y, Ali MRK, Dong B, Han T, Chen K, Chen J, Tang Y, Fang N, Wang F and El-Sayed MA, *ACS Nano*, 2018, 12, 9279–9290. [PubMed: 30118603]
12. Hung PJ, Lee PJ, Sabounchi P, Lin R and Lee LP, *Biotechnol Bioeng*, 2005, 89, 1–8. [PubMed: 15580587]
13. Gomez-Sjoberg R, Leyrat AA, Pirone DM, Chen CS and Quake SR, *Anal Chem*, 2007, 79, 8557–8563. [PubMed: 17953452]
14. Huh D, Matthews BD, Mammoto A, Montoya-Zavala M, Hsin HY and Ingber DE, *Science*, 2010, 328, 1662–1668. [PubMed: 20576885]
15. Maschmeyer I, Lorenz AK, Schimek K, Hasenberg T, Ramme AP, Hubner J, Lindner M, Drewell C, Bauer S, Thomas A, Sambo NS, Sonntag F, Lauster R and Marx U, *Lab Chip*, 2015, 15, 2688–2699. [PubMed: 25996126]
16. Kane RS, Takayama S, Ostuni E, Ingber DE and Whitesides GM, *Biomaterials*, 1999, 20, 2363–2376. [PubMed: 10614942]
17. Qin D, Xia Y and Whitesides GM, *Nat Protoc*, 2010, 5, 491–502. [PubMed: 20203666]
18. DuFort CC, Paszek MJ and Weaver VM, *Nat Rev Mol Cell Biol*, 2011, 12, 308–319. [PubMed: 21508987]

19. van Helvert S, Storm C and Friedl P, *Nat Cell Biol*, 2018, 20, 8–20. [PubMed: 29269951]
20. Vogel V, *Annu Rev Biophys Biomol Struct*, 2006, 35, 459–488. [PubMed: 16689645]
21. Ruprecht V, Wieser S, Callan-Jones A, Smutny M, Morita H, Sako K, Barone V, Ritsch-Marte M, Sixt M, Voituriez R and Heisenberg CP, *Cell*, 2015, 160, 673–685. [PubMed: 25679761]
22. Li W, Wang J, Ren J and Qu X, *Chem Sci*, 2015, 6, 6762–6768. [PubMed: 28757967]
23. Hernandez DS, Ritschdorff ET, Connell JL and Shear JB, *J Am Chem Soc*, 2018, 140, 14064–14068. [PubMed: 30350959]
24. Kim DH, Lipke EA, Kim P, Cheong R, Thompson S, Delannoy M, Suh KY, Tung L and Levchenko A, *Proc Natl Acad Sci U S A*, 2010, 107, 565–570. [PubMed: 20018748]
25. Theveneau E, Marchant L, Kuriyama S, Gull M, Moepps B, Parsons M and Mayor R, *Dev Cell*, 2010, 19, 39–53. [PubMed: 20643349]
26. Theveneau E, Steventon B, Scarpa E, Garcia S, Trepas X, Streit A and Mayor R, *Nat Cell Biol*, 2013, 15, 763–772. [PubMed: 23770678]
27. Shellard A, Szabo A, Trepas X and Mayor R, *Science*, 2018, 362, 339–343. [PubMed: 30337409]
28. Matsumoto K, Mizuno S and Nakamura T, *Curr Opin Nephrol Hypertens*, 2000, 9, 395–402. [PubMed: 10926176]
29. Gutierrez H, Dolcet X, Tolcos M and Davies A, *Development*, 2004, 131, 3717–3726. [PubMed: 15229174]
30. de Rooij J, Kerstens A, Danuser G, Schwartz MA and Waterman-Storer CM, *J Cell Biol*, 2005, 171, 153–164. [PubMed: 16216928]
31. Zaritsky A, Natan S, Ben-Jacob E and Tsarfaty I, *PLoS One*, 2012, 7, e44671. [PubMed: 22970283]
32. Garcia S, Sunyer R, Olivares A, Noailly J, Atencia J and Trepas X, *Lab Chip*, 2015, 15, 2606–2614. [PubMed: 25977997]
33. Jang H, Notbohm J, Gweon B, Cho Y, Park CY, Kee SH, Fredberg JJ, Shin JH and Park Y, *Sci Rep*, 2017, 8, 45844. [PubMed: 28374776]
34. Birchmeier C, Birchmeier W, Gherardi E and Vande Woude GF, *Nat Rev Mol Cell Biol*, 2003, 4, 915–925. [PubMed: 14685170]
35. Friedl P and Gilmour D, *Nat Rev Mol Cell Biol*, 2009, 10, 445–457. [PubMed: 19546857]
36. Weber GF, Bjerke MA and DeSimone DW, *Dev Cell*, 2012, 22, 104–115. [PubMed: 22169071]
37. Ng MR, Besser A, Brugge JS and Danuser G, *Elife*, 2014, 3, e03282. [PubMed: 25479385]
38. Das T, Maiti TK and Chakraborty S, *Lab Chip*, 2008, 8, 1308–1318. [PubMed: 18651073]
39. Ricart BG, Yang MT, Hunter CA, Chen CS and Hammer DA, *Biophys J*, 2011, 101, 2620–2628. [PubMed: 22261049]
40. Maruthamuthu V and Gardel ML, *Biophys J*, 2014, 107, 555–563. [PubMed: 25099795]
41. Park S, Jang H, Kim BS, Hwang C, Jeong GS and Park Y, *PLoS One*, 2017, 12, e0184595. [PubMed: 28886159]
42. Mangold S, Wu SK, Norwood SJ, Collins BM, Hamilton NA, Thorn P and Yap AS, *Curr Biol*, 2011, 21, 503–507. [PubMed: 21396819]
43. Ridley AJ, Comoglio PM and Hall A, *Mol Cell Biol*, 1995, 15, 1110–1122. [PubMed: 7823927]
44. Wu JH, Billings BJ and Balkovetz DF, *J Am Soc Nephrol*, 2001, 12, 2543–2553. [PubMed: 11729222]
45. Senthivel VR, Sturrock M, Piedrafita G and Isalan M, *Sci Rep*, 2016, 6, 39178. [PubMed: 27982133]
46. Yamada M, Tatsumi R, Yamanouchi K, Hosoyama T, Shiratsuchi S, Sato A, Mizunoya W, Ikeuchi Y, Furuse M and Allen RE, *Am J Physiol Cell Physiol*, 2010, 298, C465–476. [PubMed: 20007454]
47. Maruthamuthu V, Sabass B, Schwarz US and Gardel ML, *Proc Natl Acad Sci U S A*, 2011, 108, 4708–4713. [PubMed: 21383129]
48. del Rio A, Perez-Jimenez R, Liu R, Roca-Cusachs P, Fernandez JM and Sheetz MP, *Science*, 2009, 323, 638–641. [PubMed: 19179532]
49. Huvneers S and de Rooij J, *J Cell Sci*, 2013, 126, 403–413. [PubMed: 23524998]

50. Gomez GA, McLachlan RW and Yap AS, Trends Cell Biol, 2011, 21, 499–505. [PubMed: 21763139]
51. Butler JP, Tolic-Norrelykke IM, Fabry B and Fredberg JJ, Am J Physiol Cell Physiol, 2002, 282, C595–605. [PubMed: 11832345]
52. Trepats X, Wasserman MR, Angelini TE, Millet E, Weitz DA, Butler JP and Fredberg JJ, Nature physics, 2009, 5, 426.
53. Tambe DT, Hardin CC, Angelini TE, Rajendran K, Park CY, Serra-Picamal X, Zhou EH, Zaman MH, Butler JP, Weitz DA, Fredberg JJ and Trepats X, Nat Mater, 2011, 10, 469–475. [PubMed: 21602808]

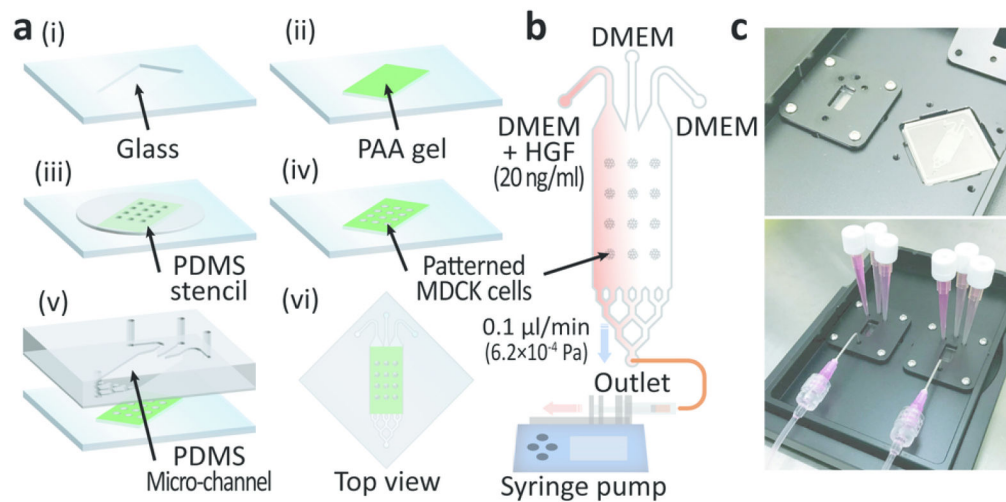


**Fig. 1.** Integrated microfluidic system with TFM. (a) A schematic of the preparation and assembly of the integrated system. Shallow-grooved glass (i) filled with fluorescent bead-embedded polyacrylamide (ii); a PDMS stencil (iii) for MDCK cell patterning with uniform size and shape; assembly of the microfluidic channel with an etched PDMS component (v) and its top view (vi). (b) Configuration and dimensions of the integrated microfluidic TFM system with an array of MDCK cell monolayers. (c) Images of the integrated system assembly (upper panel) and tubing connection (lower panel).

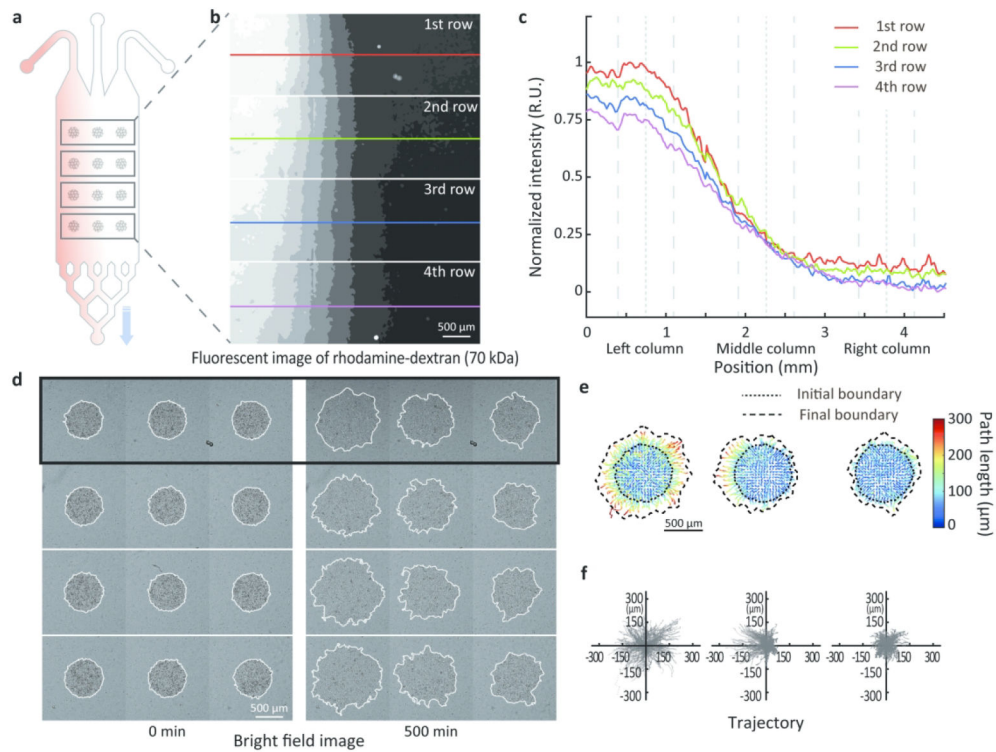


**Fig. 2.** The effect of an HGF concentration gradient on MDCK cell migration. (a) A schematic of location-specific gradients and MDCK cell island arrays. (b) The concentration gradient shown by fluorescence images of rhodamine-conjugated dextran, which has a similar molecular weight as HGF (70 kDa). (c) Fluorescence intensity profiles (colored lines in (b)) that represent various concentration gradients in microfluidic channels. (d) Bright field images of MDCK cell islands and their expansion in response to the HGF concentration over time (initial status on the left and final status after 500 min on the right). (e) Migration path and length of MDCK cells in the first row (the rectangle in (d)) shown by color coding; and boundaries at the initial status (dotted line) and final status (dashed line). (f) Trajectories of cells within the MDCK cell islands in the first row.

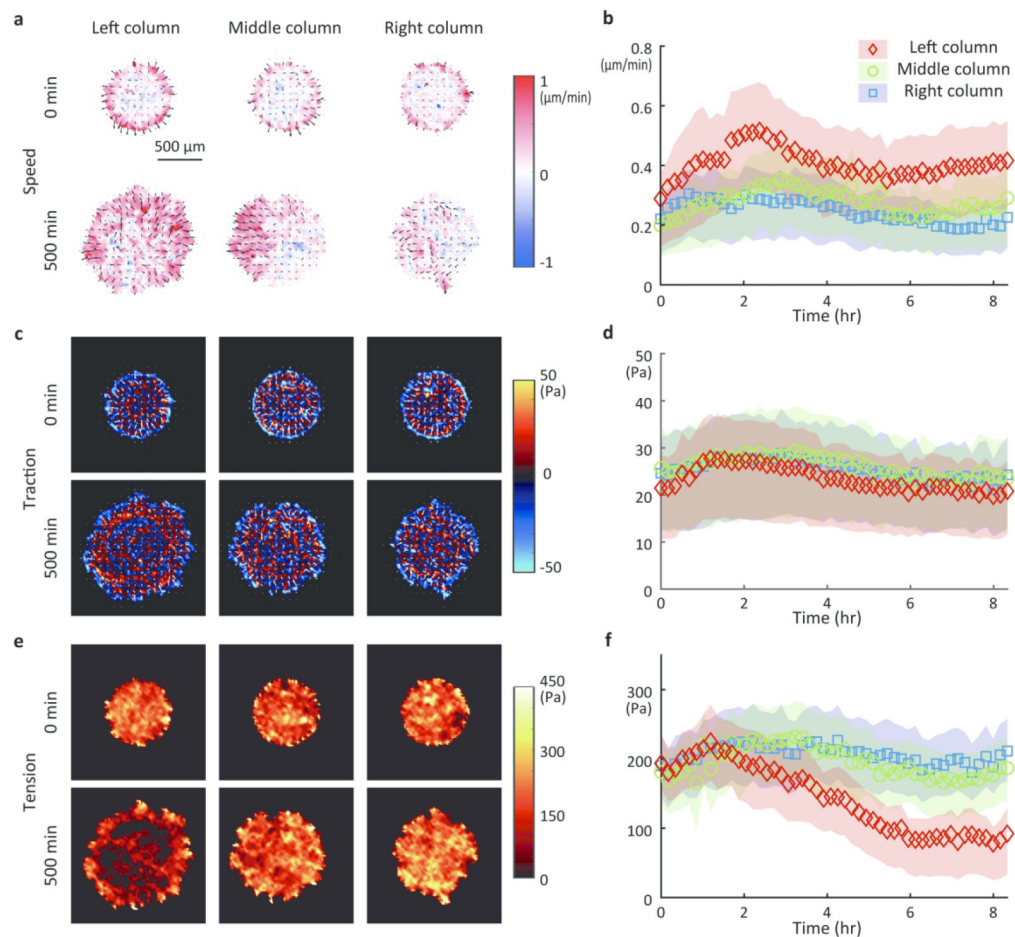


**Fig. 3.** Spatiotemporal distribution of cell migration, traction and tension in the MDCK cell islands. (a) Velocity maps of the MDCK cell islands in each column at 0 and 500 min. Color codes of radial coordinate velocity from the centroid of the cell islands, where no movement is indicated in white, outbound movement is indicated in red, and inbound movement is indicated in blue. Black arrows indicate velocity vectors. (b) Average speed of the mid-quartile (25~75%) of the MDCK cells on each island over time. (c) Traction force maps of the MDCK cell islands in each column at 0 and 500 min. Color codes of radial coordinate traction force from the centroid of each cell island, where no movement is indicated in black, outbound movement is indicated in red, and inbound movement is indicated in blue. White arrows indicate velocity vectors. (d) Average traction of mid-quartile of the MDCK cells in each island over time. (e) Tension maps of the MDCK cell islands in each column at 0 and 500 min. Color codes of tensile force, where the darkness indicates low tensile force, brightness indicates high tensile force. (f) Average tension of the mid-quartile of the MDCK cells in each island over time.

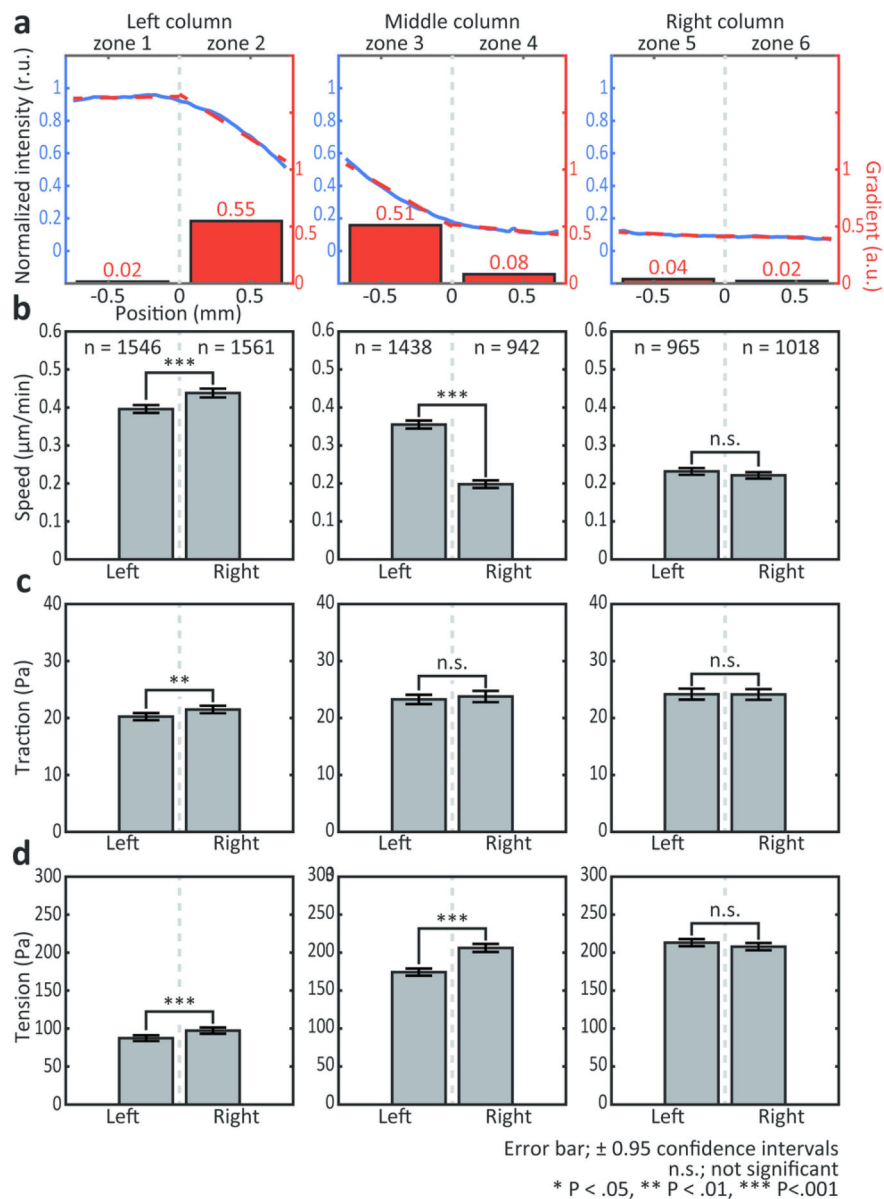


**Fig. 4.** Differential migratory behaviors of the MDCK cell islands in response to the HGF concentration and its gradient ( $t = 500$  min). (a) Estimated intensity profiles of HGF in each column (blue lines). Along the vertical centerline (gray dotted line), each column is divided by left and right sections corresponding to the left and right semicircles of the cell islands, respectively. This results in 6 zones. Intensity trend lines and their slope of each zone shown in red dashed lines and red boxes, respectively. Average cellular migration speed (b), traction force (c), and tension (d) in each zone. The number of data points is shown for each zone as follows:  $n_{\text{zone1}} = 1546$ ,  $n_{\text{zone2}} = 1561$ ,  $n_{\text{zone3}} = 1438$ ,  $n_{\text{zone4}} = 942$ ,  $n_{\text{zone5}} = 965$ , and  $n_{\text{zone6}} = 1018$ . The error bars indicate  $\pm 0.95$  confidence intervals. n.s. not significant, \*  $P < 0.05$ , \*\*  $P < 0.01$ , and \*\*\*  $P < 0.001$ .

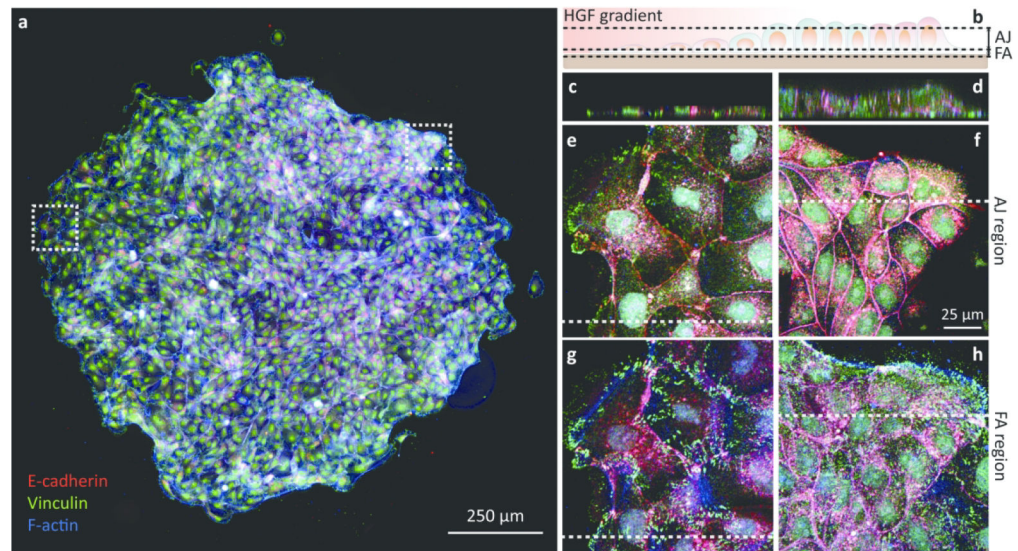


**Fig. 5.**

The HGF concentration gradient induces asymmetric distribution of actin, focal adhesions (FAs), and adherens junctions (AJs) within the MDCK cell islands. (a) Confocal fluorescence microscopy of E-cadherin (red), vinculin (green), and F-actin (blue) of a single MDCK cell island. (b) A schematic of the MDCK cell island under the HGF gradient and the regions of AJs and FAs. (c–h) Enlarged confocal microscopy images and their orthogonal views of two regions at higher and lower concentrations of HGF. Orthogonal views of a cell island at higher (c) and lower (d) HGF concentrations. Confocal microscopy images of AJ and FA regions of a cell island at the higher (e and g) and lower (f and h) HGF concentrations, respectively.